Progress in Additive Manufacturing (2023) 8:719–731
https://doi.org/10.1007/s40964-023-00450-7

FULL RESEARCH ARTICLE

Surface morphology influences of PBF-LB manufactured Ti6Al4V parts on adhesive bond strength—investigation of as-built and surface-treated conditions

Emre Ertürk[1] · Bruno Musil[1] · Gregor Diez[1] · Christian Felber[2] · Philipp Höfer[1]

Received: 7 September 2022 / Accepted: 28 April 2023 / Published online: 12 May 2023

Abstract
Additive manufacturing in combination with adhesive bonding enables high lightweight potential in structural design. A decisive factor for high adhesive bond performance are the surface properties. In the present work, the surface morphology of laser powder bed fusion (PBF-LB) processed Ti6Al4V parts was investigated in the as-built condition for the build orientations 0°, 45°, 90°. Furthermore, subsequent surface treatment by grit blasting or laser treatment allowed to modify the surface morphology and examine its effect on the bond strength. The surface characteristics were assessed using scanning electron microscopy, laser confocal microscopy and contact angle measurements. Evaluating the bond strength was done for tensile loading by centrifugal adhesion testing. The lowest bond strength was found for 0° oriented specimens, while the 45° and 90° oriented samples showed similar strengths. Fracture surface analysis of the as-built surfaces showed that the partially melted particles remain attached and cause mechanical interlocking. Furthermore, surface treatment by grit blasting allowed a minor improvement of the bond strength, while with laser treatment a significant increase was possible.

Keywords Adhesive bonding · Additive manufacturing · Surface morphology · Surface treatment

1 Introduction

As the productivity of 3D-printers continues to improve, additive manufacturing (AM) is becoming increasingly used in lightweight construction. A main advantage of AM is the high design freedom, which allows to manufacture load path optimized structures with a high degree of system integration. This enables a material efficient part design [1]. A commonly used material for metal-AM is the titanium alloy Ti6Al4V. It offers an excellent strength to weight ratio, good corrosion resistance and temperature stability and is, therefore, widely used in aerospace applications. To fully benefit from the high lightweight potential of additive manufactured titanium parts, it is necessary to also consider the joining process for the assembly design [2]. In conventional lightweight constructions with titanium, joining is often carried out by bolting and riveting, thus leaving room for further improvement. A suitable joining method for lightweight construction is adhesive bonding. The advantages compared to a mechanical joint include lower weight penalty, a more uniformly load transfer, not damaging the base material and in case of metals avoiding contact corrosion [3]. However, a common problem is that the load-bearing capability of an adhesive bond is often limited due to local stress concentrations in the bond. These stress concentrations cause premature failure and are often a result of large stiffness gradients between the joining partners [4]. With AM, the stiffnesses of the joining partners can be adjusted to achieve minimal load concentrations in the adhesive bond [5]. Therefore, the combination between AM and adhesive bonding seems promising.

This type of process combination is investigated in the research project BLANCA in the context of load introductions in sandwich structures. The project's main goal is to optimize the load introduction using AM to manufacture optimized load introduction elements and adhesive bonding to join them with the sandwich structure. The present paper is part of the project work on adhesive bonding of AM parts.

✉ Emre Ertürk
emre.ertuerk@unibw.de

[1] Institute of Lightweight Engineering, Universität der Bundeswehr München, Neubiberg, Germany

[2] Institute of Materials Science, Universität der Bundeswehr München, Neubiberg, Germany

A decisive factor for the adhesive bond performance are the surface properties. Most materials are in the untreated state not suitable for adhesive bonding. Therefore, surface treatment takes an essential role in high-performance bonding. A basic step in surface preparation is cleaning the substrate surfaces from contaminations and loose oxide layers. This is a crucial step to avoid weak boundary layers and achieve sufficient wetting of the surface by the adhesive. The simplest method to remove surface contaminations is degreasing. For organic impurities, cleaning with solvents is usually sufficient, while for strong contaminations on metals more intensive cleaning is required [6]. This is possible with physical treatment methods like laser ablation, plasma treatment and UV/Ozone treatment. These methods are not only used for cleaning, but also for modifying the surface properties. Adapting the surface chemistry to the adhesive type and creating surface roughness at the micro and nanometer scale are further steps that contribute to a high bond strength. In a study by Akram et al. [7], titanium surfaces were pretreated with atmospheric pressure plasma and evaluated for bonding with high temperature resistant polyimide adhesive in tensile shear tests. It was found that plasma treatment allows a significant improvement of the static bond strength. An important advantage of plasma treatment is the environmental friendliness, but the pretreated surfaces often require primer application due to high degradation rate when exposed to atmospheric environment [8]. A simple way of creating surface roughness at the macro- and microscopic level are mechanical surface treatments. Processes such as grit blasting are used to increase the effective contact area for bonding and to clean the surface to a certain extent. However, it is rather difficult to create desirable interlocking-features with mechanical treatment. In addition, the effectiveness of macro- and microroughness is significantly lower compared to roughness in the nanometer scale [4]. In aerospace, electrochemical processes such as phosphoric acid anodizing (PAA) are, therefore, often used for surface treatment of metals. PAA creates a thin oxide layer consisting of structures in the nanometer scale on the surface. This nano-porous layer provides a high contact area, promotes high capillary forces and allows a durable adhesive bond under environmental influences [4, 9]. However, the disadvantage of electrochemical processes is that they are environmentally unfriendly. A more sustainable method to create nano-porous layers is laser treatment. Specht et al. [10] investigated the adhesive bond performance of conventionally manufactured Ti6Al4V-samples after laser treatment. They showed that a laser induced nano-porous oxide layer improves the tensile shear strength and allows durability under hot-wet ageing. An increase of the shear lap bond strength up to 4.5 times was observed in a study by Cakir [11] for laser treatment of Ti6Al4V-sheets. A limitation of laser treatment is its tendency to produce an uneven oxide layer on the surface, with most of the oxide concentrated at the edges of the laser pulses. This has been shown in previous studies, such as Schneider and Wrobel's [12] work on a magnesium alloy treated with a ND:YAG-Laser. Optimizing the laser settings is, therefore, necessary to produce a predominantly uniform oxide layer. Additionally, the surface roughness must be kept as low as possible to improve fatigue behavior [13–15]. Furthermore, it has to be considered that laser treatment can cause residual tensile stresses in the near-surface area, which often deteriorate fatigue properties. Taube et al. [15] investigated the residual stresses in Ti6Al4V substrates caused by laser treatment for different laser intensities. They showed that at high laser intensities, the residual tensile stresses promote crack initiation. The laser treatment should, therefore, be conducted with the minimum possible laser intensity at which the oxide layer is still formed. In the present study, PBF-LB-processed Ti6Al4V samples are laser treated to examine the potential improvement in adhesive bond strength. Furthermore, surface treatment by grit blasting was also considered since it's a frequently used postprocessing step for PBF-LB-processed metallic parts.

Parts manufactured by PBF-LB have rough 'as-built' surfaces due to semi-sintered or partially melted particles [16]. The surface morphology is determined by the build parameters as well as by process-related effects. A comprehensive literature review on this topic was carried out in [17]. The build orientation is cited as an important parameter. A comparatively higher roughness is observed for inclined surfaces. This is mainly caused by a higher number of adhering particles from the powder bed and by stair-step structuring of the surface due to layer-wise production. Furthermore, a distinction is made between the upskin and downskin surface of inclined parts. The downfacing side is significantly rougher, since there is more adjacent powder that can be partially melted and due to a larger melt pool size caused by slower heat dissipation [18].

In several studies [19–21] it was shown, that the inherent roughness of AM-Ti6Al4V has a high bonding ability for static loading cases. Tensile shear testing of Ti6Al4V-PEEK joints in [19] showed that the adhesive bond strength with as-built Ti6Al4V surfaces produced by electron beam melting is comparable to laser structured surfaces. Nguyen et al. [20] conducted fracture toughness testing for metal–metal and metal–composite joints and found that the microroughness features on PBF-LB-processed Ti6Al4V surfaces can allow high adhesive bond performance. The build orientation influence on the adhesive bond performance was examined by Rodriguez et al. [21] for metal–metal joints with PBF-LB-processed Ti6Al4V parts. They evaluated the bond strength for the build orientations 0°, 45° (downskin) and 90° by means of butt joint testing. The results showed that the applied acetone cleaning was insufficient for the surface

with the highest roughness, here the 45° downskin surface. The lowest tensile strength was, therefore, measured for this surface. Only after UV/Ozone cleaning did the 45° and vertically oriented surfaces show comparable bond strengths, while for the horizontally oriented samples a slightly lower bond strength was found. The measured bond strengths are significantly influenced by the cleaning method and by the defined manufacturing parameters. Therefore, the build orientation influence was investigated in the present study for other manufacturing conditions and a different cleaning process. An overview of this work is illustrated in Fig. 1. The build orientation comparison was extended in this study by including the 45° upskin surface. Furthermore, the effect of surface treatment on the bond strength was examined for grit blasting and laser treatment. The surfaces were characterized by Scanning Electron Microscopy (SEM), Confocal Laser Scanning Microscopy (CLSM) and contact angle measurements. Afterwards, the adhesive bond performance for each surface was investigated for tensile loading.

2 Experimental

2.1 Manufacturing

Small plates with a length and width of 25 mm and a thickness of 4 mm were used as specimens in this study. Manufacturing was conducted by the project partner GERG on a Concept Laser M2 machine using standard parameters for Ti6Al4V Grade 23. For the scanning strategy a 45° stripes pattern was defined. The powder used fulfils the ASTM F3001 specification. It was supplied by GE Additive with a particle size range of 10–45 µm. After the build process, the specimens were stress relief heat treated under argon environment. In the next steps, the specimens were separated from the build plate using EDM Cutting and were then ultrasonically cleaned with deionized water to remove loose particles. Afterwards, ultrasonic cleaning with acetone was conducted to remove surface contaminations.

2.2 Surface treatment methods

2.2.1 Grit blasting

The specimens were grit blasted in a Peenmatik 1300 SDK (iepco, Switzerland) using silicon carbide as a blasting agent with a grain size range of 212–300 µm. Silicon carbide was selected since it's a standard blasting agent used in post-processing for AM. Alternatives are discussed in the results section. The grit blasting device was operated manually with a blasting angle of about 90°, a pressure of 3 bar and a nozzle size of 10 mm. The surfaces were blasted from a 20 cm distance for approximately 10 s until a uniform surface finish was achieved. Afterwards, ultrasonic cleaning was conducted to remove abrasive residues.

2.2.2 Laser treatment

The laser treatment was conducted on a TRUMPF Trumark Station 5000 marking laser system (TRUMPF, Germany) with a pulsed ND:YAG-Laser ($\lambda = 1064$ nm, $P_0 = 15$ W). The laser spot diameter was set to 30 µm using a lens with a focal length of 100 mm. All laser settings were adapted with the goal to create pronounced nanoroughness on the surface of Ti6Al4V. This was achieved with a laser power level of 35%, a scan speed of 0.4 m/s and a pulse frequency of 20 kHz. For the laser scanning strategy, a horizontal line pattern was

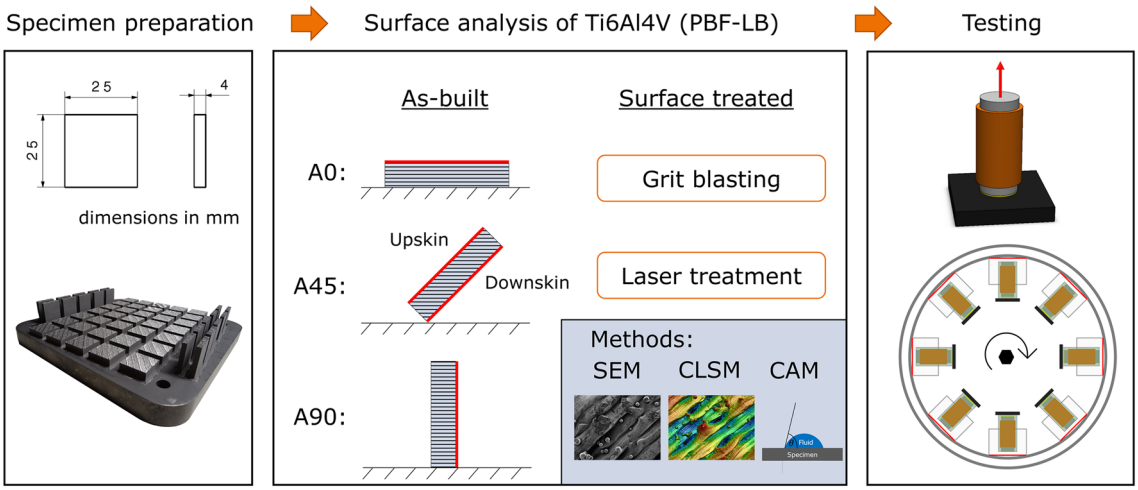

Fig. 1 Overview of the experimental investigations

defined with a laser track distance of 30 µm. With these settings, the laser scanned once over the entire surface.

2.3 Analytical methods

2.3.1 Surface morphology

Characterizing the surface textures was done in a first step by Scanning Electron Microscopy (SEM). The images were taken on a Zeiss Ultra 55 (Carl Zeiss, Germany) with a Secondary Electrons Detector (SE2) and an accelerating voltage of 1.0 kV. Quantitative information about the surface morphologies was obtained by Confocal Laser Scanning Microscopy (CLSM) using a Keyence VK-X3000 (Keyence International, Belgium). With CLSM, the height information of the topographies as well as the roughness values were determined. For each surface type at least five measurements were conducted on different locations and samples.

2.3.2 Contact angle measurement

The macroscopic wettability of the surfaces was examined by contact angle measurements using a DSA100E Drop Shape Analyzer (Krüss, Germany). First, the samples were ultrasonically cleaned with acetone. Afterwards, the measurements were conducted using the sessile drop method according to DIN EN ISO 19403–1 [22]. The contact angle is calculated by curve fitting the drop shape and averaging the contact angle measured at the ends of the droplet. As test liquids, deionized water and di-iodomethane were used in a quantity of 3 µl per drop. For each surface type at least five measurements were performed.

2.4 Adhesive joint preparation and testing

The adhesive bond performance was assessed for tensile loading by centrifugal adhesion testing (CATT). This test method is an alternative to classical butt-joint testing in a tensile testing machine. It allows time- and material-efficient testing. In this work, CATT was chosen since it is a preeminent testing method to investigate the adhesion strength. Moreover, it allows a uniform loading of the adhesive bond, which is in case of the highly irregular surfaces of PBF-LB-processed Ti6Al4V advantageous to reduce scattering of the bond strength results. In a first step, the samples were ultrasonically cleaned with acetone. After that, they were bonded with an aluminum test stamp using a bonding fixture to ensure alignment of the substrates. The bond surface of the test stamp was laser treated to avoid adhesive failure on the test stamp side. Thus, failure occurred either by cohesive failure in the adhesive or due to adhesive failure on the specimen surface. As an adhesive, the two-component epoxy adhesive Loctite EA 9395 AERO (Henkel, Germany) was used. After bonding, a test weight is screwed onto the specimen and the assembly is placed in a guide sleeve, as illustrated in Fig. 2. This setup is then finally mounted in the centrifugal testing device. In this test method, the rotational movement creates a centrifugal force, which induces a tensile loading of the adhesive bond. The load was increased linearly by 20 N/s until fracture occurred. Five tests were performed for each surface type.

3 Results and discussion

3.1 Surface morphology in as-built condition

SEM images of Ti6Al4V surfaces produced by PBF-LB are shown in Fig. 3 for the build orientations 0°, 45° and 90°. The images show the surfaces in as-built condition. The laser scanning direction is depicted for each surface. For the horizontally oriented surface A0, the main surface features are groves with an orientation of 45° and a few number of attached particles on the surface. The groves are created by the defined laser scanning pattern, while the attached particles can be caused by improper powder melting or other process related effects like the balling effect [23]. Regarding the A90 and A45-Downskin/Upskin oriented surfaces, it can be stated that the surface morphology is mainly characterized by partially melted particles. Within these three surfaces the A45-Upskin surface has the lowest quantity of attached particles, but still significantly more than on the A0 surface. A large number of ball-like particles are present on the A90 and A45-Downskin surfaces. Especially, at the downskin

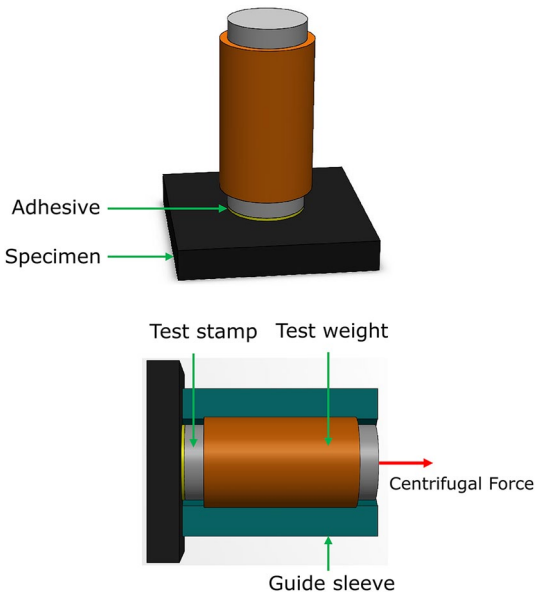

Fig. 2 Specimen setup for centrifugal adhesion testing

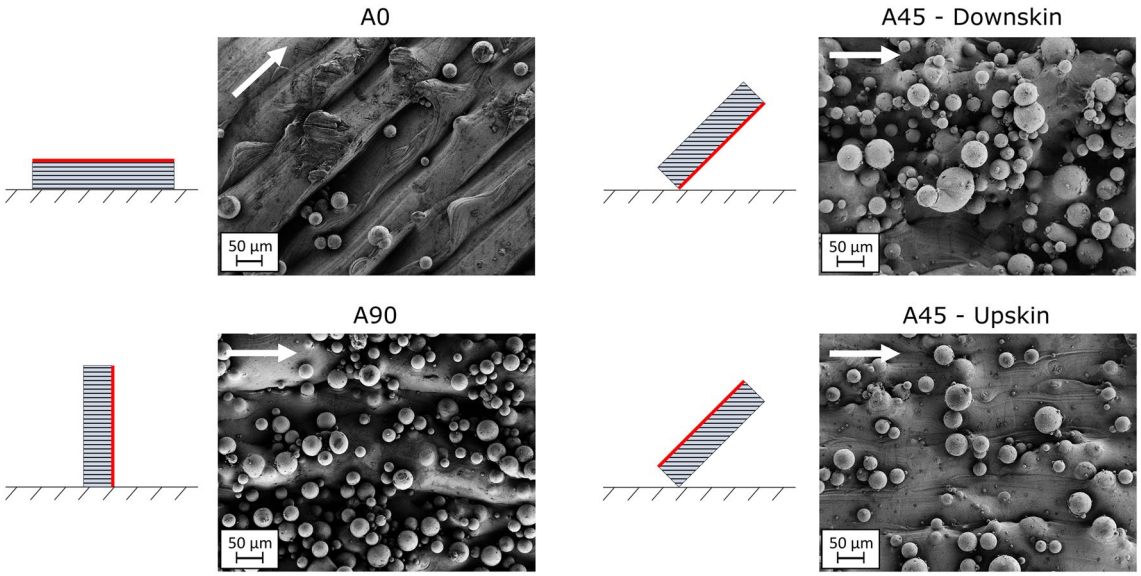

Fig. 3 SEM images of Ti6Al4V surfaces in as-built condition for the build orientations A0, A90, A45 Downskin/Upskin

surface, large particle accumulations are forming. This is caused by a slow heat dissipation at the downskin side and a high amount of adjacent particles in the powder bed [18]. Analyzing the surfaces with SEM revealed no distinct nano-roughness on the as-built surfaces.

Measurements with CLSM allowed to obtain quantitative information of the surface morphologies. The CLSM-images in Fig. 4 show the height information of the investigated surfaces. In addition, the corresponding roughness value S_a is given here, which describes the arithmetic mean roughness of a surface. Other roughness parameters which contain more specific information of certain surface aspects were also evaluated in this study. However, since S_a is still commonly used for describing the roughness, it was selected to examine its informative value for adhesive bonding. The highest roughness value was found for the A45-Downskin surface with about 21.86 µm, followed by the A90 surface. For the A0 and A45-Upskin surfaces the roughness analysis resulted in similar S_a values, which are the lowest among these surfaces. The S_a value only allows to state that the arithmetic mean roughness of the A0 and the upskin surfaces is similar. Differences in surface topography can't be expressed with this parameter. Therefore, the S_a value needs to be complemented with further roughness values or with images of the topography. For the shown surfaces, it can be concluded that the roughness is mainly influenced by the

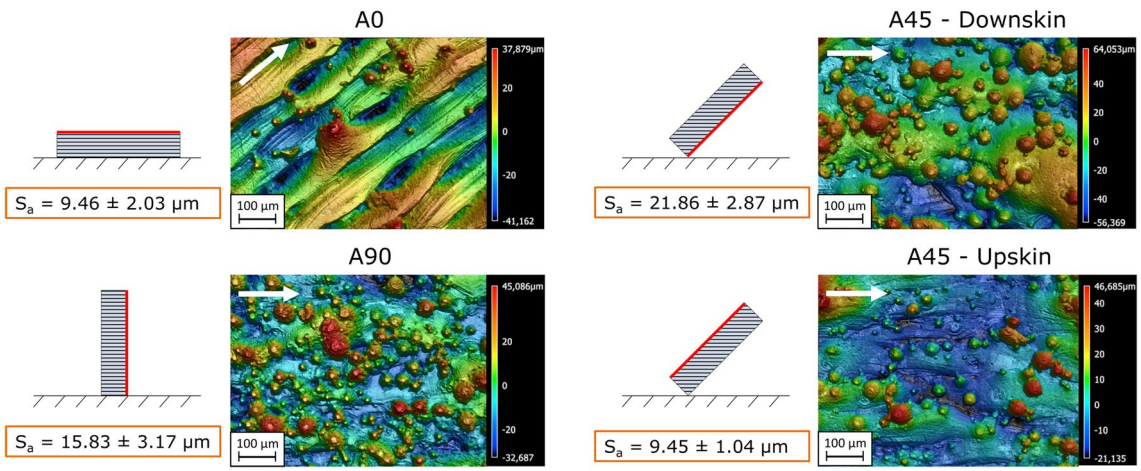

Fig. 4 CLSM images of Ti6Al4V surfaces in as-built condition for the build orientations A0, A90, A45 Downskin/Upskin and the corresponding roughness value S_a

number and size of attached particles and in case of the A0 surface by the groove structuring. Furthermore, it is interesting to note that the stair-step effect at the A45 surfaces is more pronounced on the downskin side.

3.2 Surface morphology in surface-treated condition

Surface treatment was conducted exemplary for the build orientations A0 and A90. This allowed to evaluate the surface treatment for a low and a high number of attached particles on the initial surface. CLSM images of the surface morphologies after grit blasting are shown in Fig. 5.

In case of the horizontally oriented surface A0, an increase in the mean roughness value S_a by 26.7% was observed. This is caused by texturing former smooth areas during the blasting process. For the A90 surface the roughness value was, however, decreased by around 62%, mainly due to removal of the attached particles on the surface. Furthermore, it can be stated that the topographies of both surfaces are more similar after grit blasting. Multiple areas of the grit blasted surfaces were further investigated by SEM. The images proved that residuals of the silicon carbide particles are present on the surfaces despite cleaning in the ultrasonic bath. Figure 6 exemplary shows the blasting agent residuals on the horizontally oriented surface A0.

During the blasting process, the silicon carbide particles were crushed in different sizes and have cut into the Ti6Al4V substrate. These incised blasting particles are distributed unevenly over the entire surface, but account only for a rather small proportion of the total substrate surface. However, it should still be considered that the grit blasting residues can influence the wettability of the surfaces and the adhesive bond strengths. Particularly under dynamic loads, the incised particles can cause crack initiation due to notch effects and thus worsen the fatigue performance. This

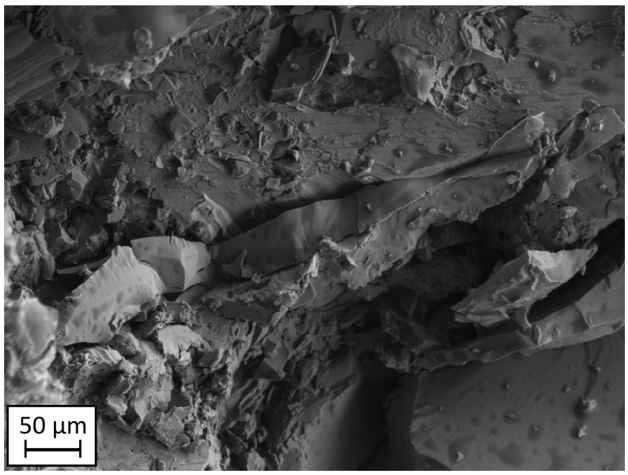

Fig. 6 Residuals of silicon carbide particles on a A0-oriented Ti6Al4V surface after grit blasting

was observed by Bagehorn et al. [14] during fatigue tests with PBF-LB-processed Ti6Al4V parts after grit blasting with corundum. Moreover, it can be noted that grit blasting mainly modifies the microroughness on the surface without generating a pronounced nanoroughness. In contrast, laser treatment allows to create roughness in two distinct scales. In the micrometer scale, the surface topography is mainly characterized by the laser pulses, as illustrated in Fig. 7 for the A0 and A90 build orientations.

Laser treatment of the A0 surface increased the mean roughness value S_a by around 50%, while a decrease of 35% was observed for the A90 surface. This decrease is due to the deformation of the attached particles on the surface caused by the laser pulses. As a result, the A0 surface shows a higher S_a value than the A90 surface after laser treatment. In addition to the microroughness it was possible to create a laser induced nano-porous layer on the surface.

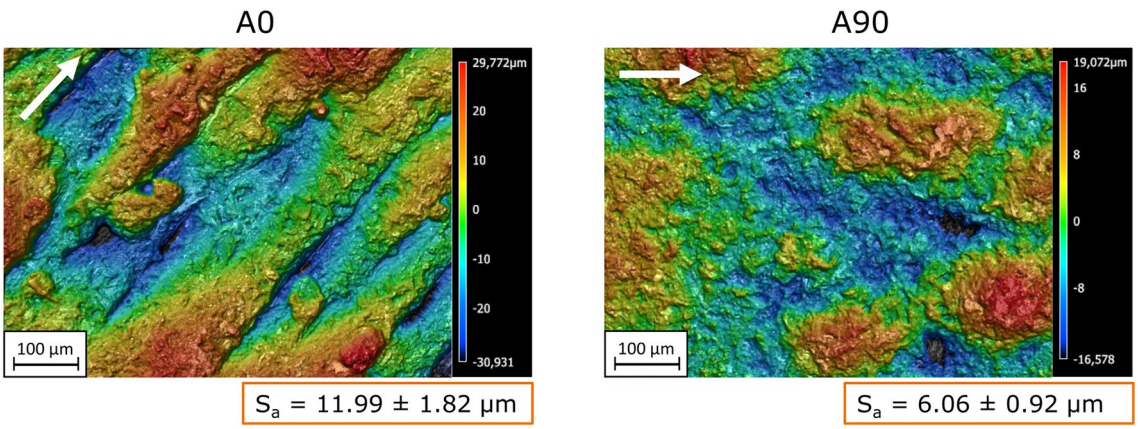

Fig. 5 CLSM images of Ti6Al4V surfaces after grit blasting for the build orientations A0, A90 and the corresponding roughness value S_a

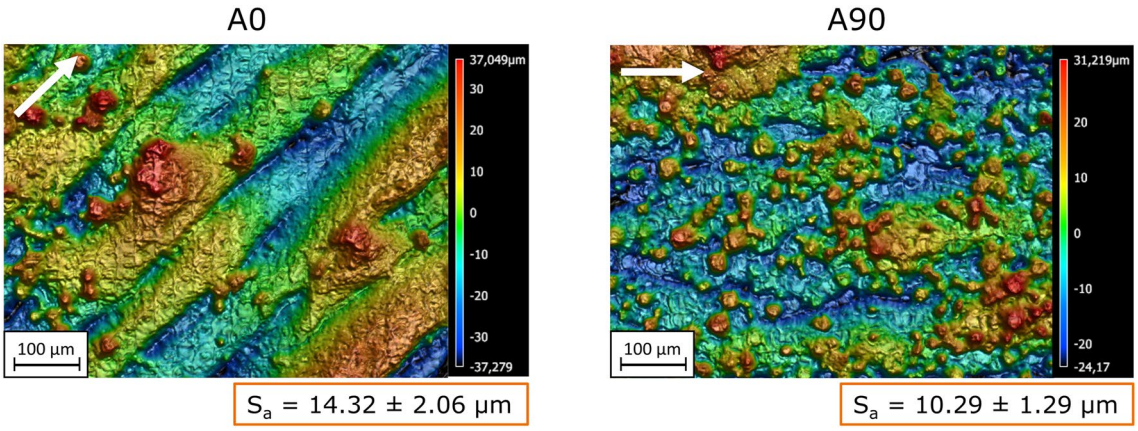

Fig. 7 CLSM images of Ti6Al4V surfaces after laser treatment for the build orientations A0, A90 and the corresponding roughness value S_a

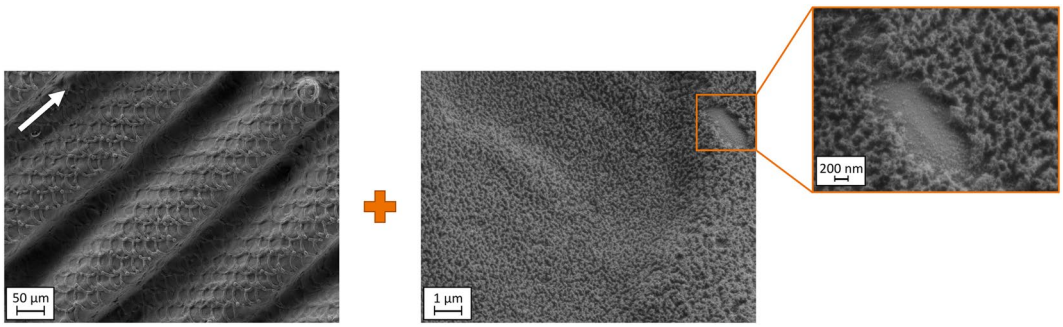

Fig. 8 SEM images of a A0-oriented Ti6Al4V surface after laser treatment

The microroughness created by the laser pulses is therefore superimposed by a pronounced nanoscale roughness. This is illustrated in Fig. 8 exemplary for a laser treated A0 surface. The nanoroughness layer has a thickness of 100–200 nm and consists of fine structures in the nanometer scale. In this study, no analysis was performed on the surface chemistry, but based on other investigations [10, 11] with a similar laser intensity it is assumed that the nanostructures are part of a TiO_2 layer. Regarding the adhesive bond performance, it was expected that the laser induced nanoroughness will cause a significant improvement in bond strength.

A comparison of the roughness S_a for the investigated surface topographies is shown in Fig. 9, including a reference value for a milled Ti6Al4V surface. In this study, a total of eight different surface topographies of PBF-LB-processed Ti6Al4V were considered, not counting the reference surface. The S_a value for these surfaces ranged from approximately 6 to 22 µm. The lowest roughness value was found for the A90 surface after grit blasting, which is still considerably higher than that of the milled reference surface. In contrast, the A45 downskin surface in the as-built condition showed the highest S_a value. It is important to note that the

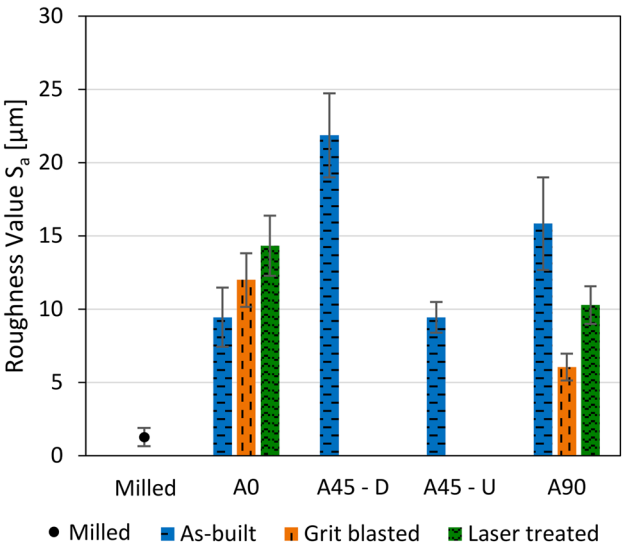

Fig. 9 Averaged roughness value S_a, shown for the different build orientations in as-built and surface-treated conditions. The results for a milled surface are also shown as a reference

S_a value characterizes the microroughness of the examined surface topographies. However, for evaluating the adhesion strength, it is essential to also consider the nanoscale roughness. In the present study, only the laser-treated surfaces showed a pronounced nanoroughness.

3.3 Surface wettability

In a study by Rodriguez et al. [21], contact angle measurements with deionized water were used to characterize the macroscopic wettability of PBF-LB-processed Ti6Al4V. The results indicated a correlation between the macroscopic contact angle and the adhesive bond strength of metal–metal joints bonded with an epoxy adhesive. However, based on the findings in [24, 25] it can be assumed that the macroscopic contact angle does not correlate with the adhesive bond strength. Given these discrepancies, the present study includes contact angle measurements to investigate the relation between macroscopic contact angles and adhesive bond strength. Moreover, performing the contact angle measurements allowed to assess the effectivity of the applied cleaning process, as this method is very sensitive to surface contaminations. Measuring the contact angles on the macroscopically rough surfaces required to adapt the volume of the liquid droplet. Initial measurements with 2 µm water drops resulted in highly irregular droplet shapes. After increasing the water drop volume to 3 µm approximately round droplets could be created on the surfaces, which allowed to measure the contact angles. However, it is important to note that the contact angles measured on rough surfaces have to be considered as approximations, since an exact measurement with the sessile drop method requires a macroscopically flat surface [25]. In case of highly anisotropic surfaces, the contact angles are also influenced by the anisotropy. In this work, the surface direction dependence of the contact angles was investigated for the highly anisotropic surface A0 in the as-built condition. This surface shows a pronounced anisotropy due to the groves on the surface induced by the defined laser scanning pattern. When applying a water drop on this surface, the droplet is aligning along the groves, resulting in an elliptical drop shape, as illustrated below. The contact angles were measured in the surface directions 0°, 45° and 90° relative to the groves on a defined surface spot. Figure 10 illustrates the contact angle measurements.

The elliptical drop shape causes varying contact angles along the different surface directions. Evaluating the mean contact angle of each direction after multiple measurements showed that the contact angles vary in the range of 48° to 62° on the evaluated spot. This implies a reasonable dependence of the measured contact angle on the surface direction. For a detailed comparison of the macroscopic wettability, this dependence has to be considered. In the present work, however, the anisotropic influence can only be evaluated for a subset of the investigated surfaces, namely "A0-as built", "A0-grit blasted" and "A90-grit blasted", since complete macroscopic wetting was observed for all the other considered surfaces. Furthermore, the macroscopic wettability of the surfaces is assessed only qualitatively due to the increased uncertainty when applying the contact angle measurement method to macroscopically rough surfaces [25]. Therefore, the surface direction dependence was not further investigated in this study.

The contact angles measured with deionized water for the investigated surfaces are shown in Fig. 11. In addition, the contact angle of a milled Ti6Al4V surface is depicted as a reference. It is important to note that the measured contact angles only describe the macroscopic wettability. The horizontally oriented surface A0 has a lower contact angle than the milled surface, thus showing better macroscopic wettability with deionized water. However, comparing the A0 surface with the other build orientations in the as-built condition shows that its macroscopic wettability is significantly worse, since for the 45° and 90° surfaces complete macroscopic wetting was observed. All samples were manufactured with the same process parameters and using the same inert gas. Therefore, it can be assumed that differences in surface chemistry can be neglected for the as-built surfaces. This leaves the surface topography as a main reason for the lower wettability of A0. A main difference in topography is that the A0 surface has the

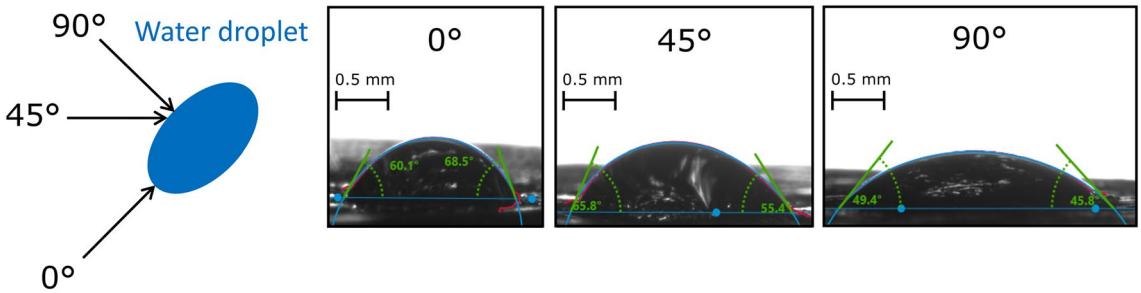

Fig. 10 Contact angle measurements on a A0-oriented Ti6Al4V surface in as-built condition. Contact angles are measured in the surface directions 0°, 45° and 90° relative to the surface groves

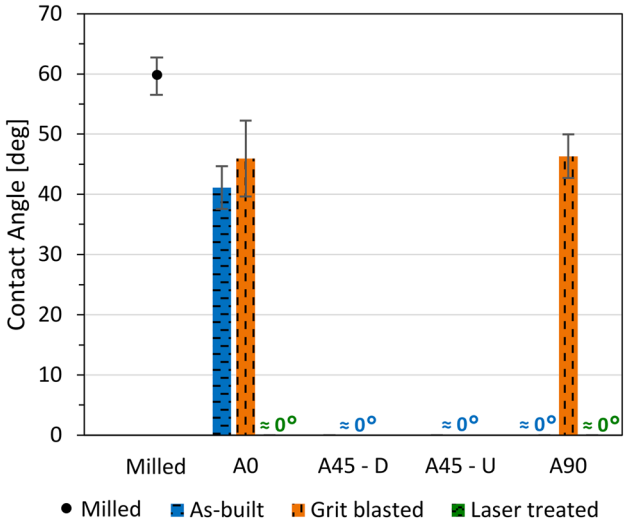

Fig. 11 Contact angles measured with deionized water, shown for the different build orientations in as-built and surface-treated conditions. The results for a milled surface are also shown as a reference

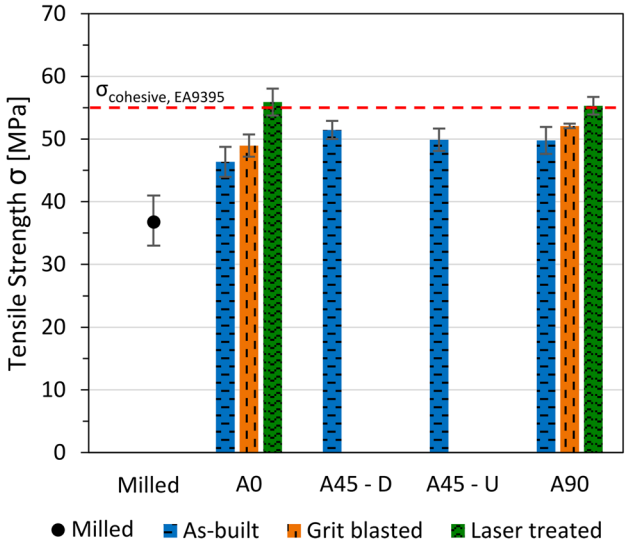

Fig. 12 Adhesive bond strength for tensile loading, shown for the different build orientations in as-built and surface-treated conditions. The results for a milled surface are also shown as a reference

lowest quantity of attached particles. It could therefore be assumed, that a higher number of ball-like particles can have a positive effect on the macroscopic wettability. However, a requirement for this is that the applied cleaning method is sufficient to remove contaminations on the surface. Especially at highly structured surfaces like A45-Downskin there is a risk that contaminations remain in the surface textures, which could cause poor wetting. This happened in [21], where due to improper cleaning the highest contact angle among the as-built Ti6Al4V surfaces was measured for the A45-Downskin surface. The measurements in the present study indicate that ultrasonic cleaning with acetone seems to be a sufficient cleaning process since complete macroscopic wetting was observed for the highly textured A45-Downskin surface.

Grit blasting resulted in an increase in the contact angle for the as-built surfaces, especially for A90. Thus, it can be assumed that grit blasting reduces the macroscopic wettability with a polar component. The wettability with a disperse component was also investigated in this study. It was observed that grit blasting only has a minor influence on the contact angles measured with di-iodomethane. It was, therefore, concluded that the overall macroscopic wettability is worsened by grit blasting. One reason for this could be that the oxygen content on the surface is decreased by grit blasting due to damaging the native oxide-layer of Ti6Al4V, as it was observed by Rodriguez et al. [26] and Brack [27]. Another reason could be the presence of blasting agent residues on the surface. Furthermore, it was found that after laser treatment all surfaces show complete macroscopic wetting. This can be attributed to the laser induced nano-porous layer on the surface.

3.4 Centrifugal adhesion testing

The adhesive bond strengths for tensile loading obtained by centrifugal adhesion testing are shown in Fig. 12. The cohesive strength of the used epoxy adhesive EA9395 [28] and the tensile strength for a milled Ti6Al4V surface are also depicted in this chart. It should be noted that all samples were ultrasonically cleaned with acetone before adhesive bonding.

The results show that all as-built surfaces are performing better than the milled surface, with a 25–35% higher tensile strength. Within the as-built surfaces, the lowest tensile strength was found for the horizontally oriented surface A0, while the A45 and A90 surfaces showed similar strengths between 50 and 51.5 MPa. Comparing the bond strengths with the average roughness value S_a of the surfaces shows, that a higher roughness in terms of the S_a value doesn't indicate a higher bond strength. This shows that it is not useful to describe the surface roughness only with the S_a value and to use this for assessing the potential adhesive bond performance. However, this is still an often used approach. Evaluating the surface topography shows that the surface with the lowest quantity of partially melted particles, here A0, also has the lowest bond strength. It can be therefore assumed, that a certain increase in particle numbers on the surface can have a positive effect on the bond strength. The particles increase the surface area and can also cause interlocking. Requirements for interlocking are that the particles don't break off from the base material and that the adhesive can flow around the particles. This was proven for the used epoxy adhesive by evaluating the fracture surfaces

using SEM. Figure 13 shows the fracture surface of a A0 surface in an area where adhesive failure occurred. It was observed that partially melted particles remain attached to the surface. This means, that the bond between particle and base material is stronger than the adhesion strength of the surface. Furthermore, it was found that adhesive residues are present around the particles, which indicates local interlocking. Nguyen et al. [20] also found that the attached particles remain on the surface for mode I static fracture toughness testing using a two component epoxy film adhesive. The stress loading in these tests is, however, much lower than in the tensile tests performed in the present study. The bond strength of the particles could, therefore, be further quantified with the shown results.

The results of the grit blasted samples show that the adhesive bond strength could be slightly increased, although grit blasting reduced the macroscopic wettability as shown by the contact angle measurements. This means that the bond strengths do not correlate with the measured contact angles. This is consistent with studies on polymer substrates [25], but contrary to what Rodriguez et al. [21] found in their investigation of the adhesive bond strength of PBF-LB-processed Ti6Al4V parts. In their study, the adhesive bond strengths were in line with the contact angle measurement results. It was found that the adhesive bond strength is higher for a lower contact angle of the surface. However, the results for grit blasting in the present study indicate that the adhesive bond strength is not in line with the contact angles. The problem with standard contact angle measurements is that only the macroscopic wettability is characterized. However, the relevant order of magnitude for adhesion is in the sub-micrometer scale. It is, therefore, not suitable to assess the adhesion strength of a surface with macroscopic contact angles [24]. This is also shown by the results in this study. Evaluating the surface topography by analyzing the surface features seems to be a more reliable approach, since it is known that roughness, especially in the nanometer scale, and interlocking have a major influence on the adhesive bond performance of metal joints [4]. Due to different effectiveness, it is important to distinguish between roughness in nano-, micro- and macro-scale. In case of grit blasting, the slight increase in tensile strength could be caused by roughening former smooth areas. The minor improvement can be explained by the fact that mainly microroughness is created, which contributes less to adhesion than nanoscale roughness. To improve the adhesive bond performance a different blasting agent could be used. For example, the SACO® process uses silane-coated corundum, which allows an in situ coating during the blasting process. This coating enhances the durability of the adhesive bond [6]. An application of the SACO® process for PBF-LB-processed Ti6Al4V parts needs to be investigated.

An increase in tensile strength by 8–20% was achieved by laser treatment. This increase can be attributed to the laser-induced nano-porous layer on the surface. However, the improvement of the bond strength by laser treatment was limited here for both built orientations A0 and A90 by the cohesive strength of the used epoxy adhesive. The real adhesion strength of the laser treated surfaces could, therefore, be even higher. The results confirm, that nanoroughening causes a more pronounced improvement than modifying the microroughness features on the surface. Evaluating the fracture surfaces also showed the effectiveness of laser treatment. In Fig. 14, the fracture surfaces are exemplarily shown for the horizontally oriented surfaces A0. It should be noted that the same fracture modes were also observed for the A90 build orientation.

In as-built condition the failure occurs in mixed mode, i.e., partial cohesive failure and partial adhesive failure at the surface of the specimen. Analyzing the fracture surface with SEM revealed that areas with more particles tend to show cohesive failure. This can be explained by an increased surface area and local interlocking of the adhesive close to the particles. Moreover, it was found that the

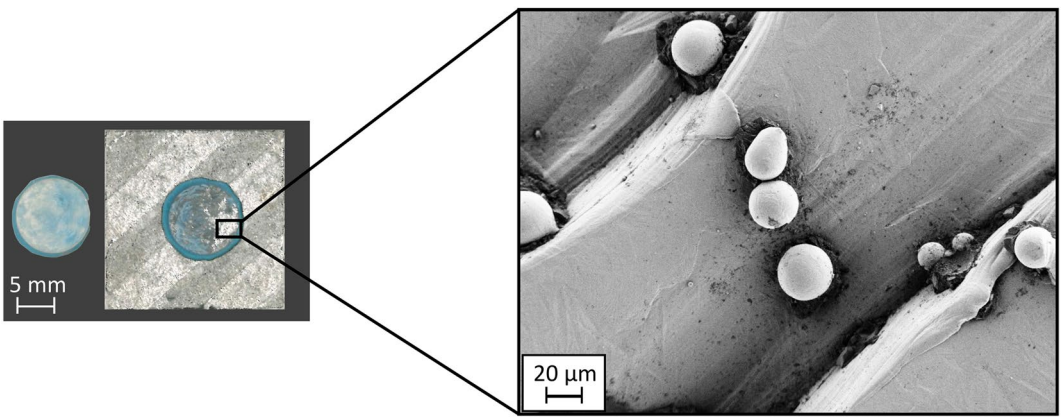

Fig. 13 Fracture surface of a A0 sample analyzed by SEM in an area of adhesive failure

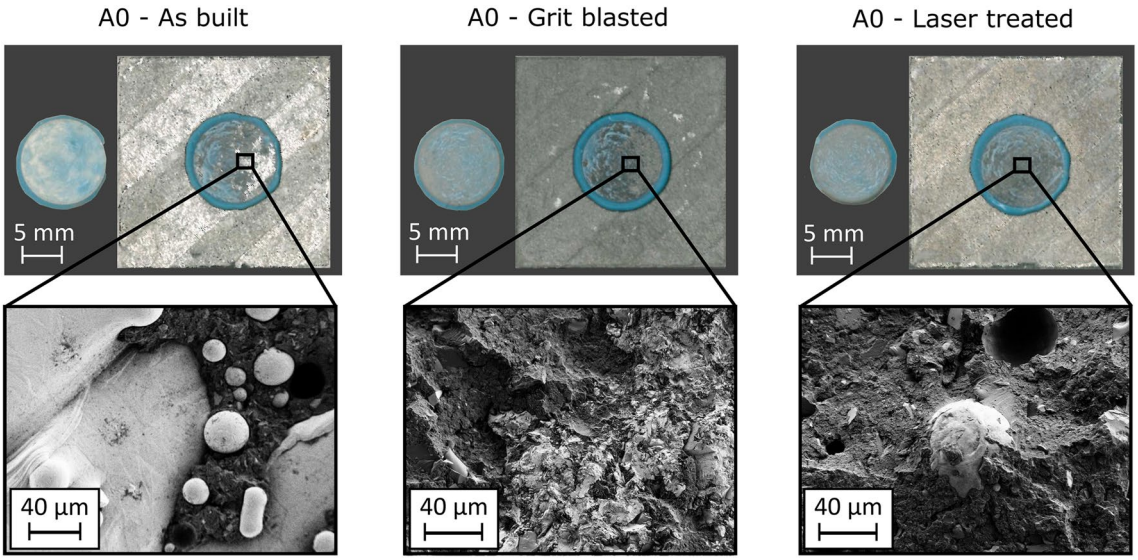

Fig. 14 Fracture surfaces for the build orientation A0 in as-built and surface-treated conditions

upper surface of the particles shows almost no adhesive residues. This indicates an insufficient bond strength on the particles top side. One reason for this could be the missing interlocking on this side of the particles. Grit blasting the A0-surface resulted in the same mixed failure mode. Compared to the as-built surface, the proportion of the two failure modes is similar. The adhesive residues and the grit blasted surface appear in the same color in the SEM (SE2 detector), which makes the distinction more difficult in this case. The darker areas in the SEM image correspond to the adhesive. After laser treatment, the failure mode switched from mixed mode to almost complete cohesive failure near the surface interface. A thin adhesive layer remains on the surface that covers the laser-induced nano-porous roughness. Evaluating the fracture surface with SEM showed that few particles are present with no adhesive residues on the upper side. This was only observed for a very few number of particles, which are located at elevations and have a larger size. In this case, the laser treatment couldn't create a pronounced nanoroughness on the upper surface of the particle. This can be explained by an insufficient laser intensity in these areas. Since the laser treated specimens failed after reaching the cohesive strength of the used epoxy adhesive, it can be assumed that these few local gaps in the nanoroughness layer didn't affect the adhesive bond strength for the investigated tensile loading case.

It can be concluded that the laser-induced nanoroughness layer allows a high adhesion strength. The surfaces in as-built and grit blasted condition are weaker, but with an adhesive bond strength between 46 and 51.5 MPa for tensile loading they are still on a level comparable to conventionally manufactured Ti6Al4V surfaces after grit blasting [21].

4 Conclusions

In this study, the effect of surface morphology on the adhesive bond performance of PBF-LB-processed Ti6Al4V parts was investigated for different built orientations in as-built and surface-treated conditions. The adhesive bond strength was assessed for tensile loading.

It was found that the adhesion strength of Ti6Al4V surfaces in the as-built condition shows a dependency on the built orientation. The lowest tensile strength was measured for a horizontally oriented surface, while the 45° upskin and downskin surfaces as well as the vertically oriented surface showed similar bond strengths. Aligning the parts in an appropriate build direction can, therefore, improve the bonding potential. Furthermore, it was shown that the adhesive bond strengths are not in line with the roughness value S_a of the surfaces and the contact angle measurement results. The results demonstrated that S_a-values and macroscopic contact angles are not suitable for assessing the adhesive bond strength. Evaluating the surface topography by analyzing the surface features seems to be a more reliable approach to assess the bond strength. This means to analyze the roughness shapes for assessing the interlocking potential and to evaluate the roughness distribution on the surface, as well as the roughness scales. Regarding the roughness shapes, it could be shown that the partially melted particles on the as-built Ti6Al4V surfaces can cause mechanical interlocking, since they remain

attached on the surfaces as shown by fracture surface analysis. An increase in adhesive bond strength was observed after surface treatment. Modifying the surfaces by grit blasting caused a minor improvement, while laser treatment allowed to achieve cohesive failure with an 8–20% increase in tensile strength. The results show the different effectiveness of micro- and nanoroughness. Grit blasting mainly causes microroughness, whereas with laser treatment a more effective nanoroughness can be created on the surface. It can be concluded that the inherent roughness of PBF-LB-processed Ti6Al4V surfaces shows a bonding potential that is comparable to grit-blasted surfaces. Laser treatment has been found to significantly enhance the adhesive bond strength by inducing nanoroughness on the surface. A cost efficient application of laser treatment could be to use it only for partial activation of surfaces in areas where stress concentrations in the adhesive bond are expected. In future work, the surface morphology influences need to be investigated for other static loading cases and fatigue loading. Especially for fatigue loading a significant influence of the surface morphology is expected [29]. Regarding laser treatment it is known that the laser pulses can damage the base material [15]. It is, therefore, necessary to investigate the extent to which these damages affect the fatigue behavior. In addition, the durability of the surfaces must be evaluated to define a suitable surface design for high adhesive bond performance.

Acknowledgements This study is part of the research project BLANCA, which is funded by the Bavarian Ministry of Economic affairs, Regional development and Energy (StMWi) within the program BayLu-25. We thank the partners within this research project, especially the project partner Modell- und Formenbau Blasius GERG GmbH, for manufacturing the specimens. Major part of this work was conducted in the laboratories of the Institute of Materials Science (Universität der Bundeswehr München) and the Bundeswehr research institute WIWeB. We would like to thank them for providing access to their laboratory equipment and for technical support.

Sponsored by

Bavarian Ministry of Economic Affairs, Regional Development and Energy

Funding Open Access funding enabled and organized by Projekt DEAL.

Data availability The data that support the findings of this study are available from the corresponding author upon request.

Declarations

Conflict of interest The authors declare that there is no conflict of interest.

References

1. Schwenke J, Krause D (2020) Optimization of load introduction points in sandwich structures with additively manufactured cores. Des Sci. https://doi.org/10.1017/dsj.2020.10
2. Türk DA, Kussmaul R, Zogg M, Klahn C, Leutenecker-Twelsiek B, Meboldt M (2017) Composites part production with additive manufacturing technologies. Procedia CIRP 66:306–311. https://doi.org/10.1016/j.procir.2017.03.359
3. European Cooperation for Space Standardization (2011) Space engineering Adhesive bonding handbook ECSS-E-HB-32–21A. ESA Requirements and Standards Division, Noordwijk
4. Da Silva LF, Öchsner A, Adams RD (2011) Handbook of adhesion technology. Springer, Berlin, Heidelberg. https://doi.org/10.1007/978-3-642-01169-6
5. DVS e.V. (2021) Gestaltungsempfehlungen zum Kleben additiv gefertigter Bauteile Merkblatt DVS 1401. DVS Media, Düsseldorf
6. Marques AC, Mocanu A, Tomic NZ, Balos S, Stammen E, Lundevall A, Abrahami ST, Günther R, de Kok JM, de Freitas ST (2020) Review on adhesives and surface treatments for structural applications: recent developments on sustainability and implementation for metal and composite substrates. Materials 13:5590. https://doi.org/10.3390/ma13245590
7. Akram M, Jansen KM, Ernst LJ, Bhowmik S (2011) Atmospheric pressure plasma surface modification of titanium for high temperature adhesive bonding. Int J Adhesion & Adh 31:598–604. https://doi.org/10.1016/j.ijadhadh.2011.05.009
8. Burchardt B (2010) Advances in polyurethane structural adhesives. In: Dillard DA (ed) Advances in structural adhesive bonding. Woodhead Publishing, pp 35–65
9. Nittel C (2017) Einfluss hybrider Strukturklebungen auf das Ermüdungsverhalten einer Aluminiumlegierung unter bruchmechanischer und kontinuumsmechanischer Betrachtungsweise. Dissertation, Universität der Bundeswehr München
10. Specht U, Ihde J, Mayer B (2014) Laser induced nano-porous Ti–O-layers for durable titanium adhesive bonding. Mat Sci Eng Tech 45:1116–1122. https://doi.org/10.1002/mawe.201400360
11. Cakir FH (2022) Enhancing the adhesive bonding strength of Ti6Al4V sheets with fiber laser texturing. Int J Adhesion & Adh 114:103117. https://doi.org/10.1016/j.ijadhadh.2022.103117
12. Schneider N, Wrobel C (2015) Use of high-energy laser radiation for surface preparation of magnesium for adhesive applications. Appl Adhes Sci 3:17. https://doi.org/10.1186/s40563-015-0044-2
13. Wagner L (1999) Mechanical surface treatments on titanium, aluminum and magnesium alloys. Mat Sci and Eng. https://doi.org/10.1016/S0921-5093(98)01168-X
14. Bagehorn S, Mertens T, Greitemeier D, Carton L, Schoberth A (2015) Surface finishing of additive manufactured Ti-6Al-4V - a comparison of electrochemical and mechanical treatments. 6th Eur Conf Aerosp Sci.
15. Taube A, Kurtovic A, Niendorf T, Mertens T, Zinn C, Schaper M, Maier HJ (2016) Influence of surface pre-treatments on the high-cycle fatigue behavior of Ti–6Al–4V – from anodizing to laser-assisted techniques. Int J Fat 91:195–203. https://doi.org/10.1016/j.ijfatigue.2016.06.010

16. Witkin DB, Patel DN, Helvajian H, Steffeney L, Diaz A (2019) Surface treatment of powder-bed fusion additive manufactured metals for improved fatigue life. J Mat Eng Perf 28:681–692. https://doi.org/10.1007/s11665-018-3732-9
17. Obilanade D, Dordlofva C, Törlind P (2021) Surface roughness considerations in design for additive manufacturing—a literature review. Proc Des Soc 1:2841–2850. https://doi.org/10.1017/pds.2021.545
18. Ilin A, Logvinov R, Kulikov A, Prihodovsky A, Xu H, Ploshikhin V, Günther B, Bechmann F (2014) Computer aided optimisation of the thermal management during laser beam melting process. Phys Procedia 56:390–399. https://doi.org/10.1016/j.phpro.2014.08.142
19. Moritz J, Götze P, Schiefer T, Stepien L, Klotzbach A, Standfuß J, Lopez E, Brückner F, Leyens C (2021) Additive manufacturing of titanium with different surface structures for adhesive bonding and thermal direct joining with fiber-reinforced polyether-ether-ketone (peek) for lightweight design applications. Metals 11:265. https://doi.org/10.3390/met11020265
20. Nguyen AT, Brandt M, Orifici AC, Feih S (2016) Hierarchical surface features for improved bonding and fracture toughness of metal-metal and metal-composite bonded joints. Int J Adhesion & Adh 66:81–92. https://doi.org/10.1016/j.ijadhadh.2015.12.005
21. Ardila-Rodriguez LA, Rans C, Poulis JA (2021) Effect of surface morphology on the Ti–Ti adhesive bond performance of Ti6Al4V parts fabricated by selective laser melting. Int J Adhesion Adh 110:102918. https://doi.org/10.1016/j.ijadhadh.2021.102918
22. Deutsches Institut für Normung e. V (2019) Beschichtungsstoffe - Benetzbarkeit - Teil 1: Begriffe und allgemeine Grundlagen DIN EN ISO 19403–1. Beuth, Berlin
23. Zhang LC, Attar H (2016) Selective laser melting of titanium alloys and titanium matrix composites for biomedical applications: a review. Adv Eng Mat 18:463–475. https://doi.org/10.1002/adem.201500419
24. Arikan ES (2020) Oberflächenmodifikation von Polyetheretherketon (PEEK) für das strukturelle Kleben in der Luftfahrt. Dissertation, Universität der Bundeswehr München. ISBN 9783843945844
25. Holtmannspötter J (2018) How surfaces of carbon fiber reinforced plastics with thermoset matrices need to be treated for structural adhesive bonding. The J of Adhesion. https://doi.org/10.1080/00218464.2018.1519702
26. Ardila-Rodriguez LA, Boshuizen B, Rans C, Poulis JA (2021) The influence of grit blasting and UV/Ozone treatments on Ti–Ti adhesive bonds and their durability after sol-gel and primer application. Int J Adhesion Adh 104:102750. https://doi.org/10.1016/j.ijadhadh.2020.102750
27. Brack N, Rider AN (2014) The influence of mechanical and chemical treatments on the environmental resistance of epoxy adhesive bonds to titanium. Int J Adhesion Adh 48:20–27. https://doi.org/10.1016/j.ijadhadh.2013.09.012
28. Henkel Corporation Aerospace (2013) Loctite EA 9395 AERO Technical Data Sheet. https://www.pccomposites.com/wp-content/uploads/2015/07/PCRS9395-QT_TDS.pdf. Accessed 11 Aug 2022
29. Thäsler T, Holtmannspötter J, Gudladt HJ (2019) Surface topography influences on the fatigue behavior of composite joints. Key Eng Mat 809:341–346. https://doi.org/10.4028/www.scientific.net/KEM.809.341